

"The submitted manuscript has been authored by a contractor of the U.S. Government under contract DE-AC05-84OR21400. Accordingly, the U.S. Government retains a nonexclusive, royalty-free license to publish or reproduce the published form of this contribution, or allow others to do so, for U.S. Government purposes."

CONF-8810231--3

CONF-8810231--3

DE89 003932

WHIST TRANSPORT ANALYSIS OF HIGH NEUTRON PRODUCTION, ICRH HEATED, PELLET FUELED JET PLASMAS*

W.A. HOULBERG, S.L. MILORA, J.S. TOLLIVER
Oak Ridge National Laboratory
Oak Ridge, Tennessee

C.K. PHILLIPS
Princeton Plasma Physics Laboratory
Princeton, New Jersey

DISCLAIMER

This report was prepared as an account of work sponsored by an agency of the United States Government. Neither the United States Government nor any agency thereof, nor any of their employees, makes any warranty, express or implied, or assumes any legal liability or responsibility for the accuracy, completeness, or usefulness of any information, apparatus, product, or process disclosed, or represents that its use would not infringe privately owned rights. Reference herein to any specific commercial product, process, or service by trade name, trademark, manufacturer, or otherwise does not necessarily constitute or imply its endorsement, recommendation, or favoring by the United States Government or any agency thereof. The views and opinions of authors expressed herein do not necessarily state or reflect those of the United States Government or any agency thereof.

MASTER

* Research sponsored by the Office of Fusion Energy, U.S. Department of Energy, under contract DE-AC05-84OR21400 with Martin Marietta Energy Systems, Inc.

DISTRIBUTION OF THIS DOCUMENT IS UNLIMITED

WHIST TRANSPORT ANALYSIS OF HIGH NEUTRON PRODUCTION, ICRH HEATED, PELLET FUELED JET PLASMAS

W.A. HOULBERG, S.L. MILORA, J.S. TOLLIVER
Oak Ridge National Laboratory
Oak Ridge, Tennessee

C.K. PHILLIPS
Princeton Plasma Physics Laboratory
Princeton, New Jersey

and the JET Pellet Injection Team

INTRODUCTION

The WHIST 1-1/2-D predictive transport code is used to model the particle and energy transport of JET pellet-fueled, ICRH-heated plasmas. Pellet injection during the current rise phase was used to produce strong central peaking of the particle density followed by central ICRH heating and led to transient period of enhanced confinement.[1] The evolution of the density profile as well as the electron and ion temperature profiles and strong ICRH heating conditions are examined during this period of enhanced confinement in the context of models for particle and energy transport.

Because WHIST is a predictive transport code, it requires models for particle and energy sources and transport coefficients. The analysis procedure thus consists of modeling the particle source terms (pellets, gas, and recycled neutrals), energy source terms (ohmic and ICRH heating), and energy loss terms (primarily radiation), and varying the transport models until the best qualitative and quantitative agreement is obtained between calculated and observed quantities. We find that plasma behavior is well described during the first second of ICRH heating following pellet injection by the same transport coefficients that describe the ohmic plasma. The distinction between electron and ion thermal losses depends on the relative heating rates of electrons and ions as determined by the ICRH model, as well as the radiation losses.

ICRH MODEL

The ICRH heating model is an extension of the PPPL ray-tracing code[2] used as a subroutine of the WHIST transport code.[3] Input from WHIST consists of plasma geometry, magnetic field, and plasma densities and temperatures. Typically, 20 rays are launched from the antenna and their propagation is followed using ray-tracing equations for a warm-fluid, multi-species plasma.[4] The initial spatial coordinates, the mode numbers, and the power content along the antenna are assumed quantities. Wave damping is calculated using the Kennel and Engelmann quasilinear diffusion operator,[5] as each ray propagates through the plasma. Then the distribution function for the resonant or minority species is evolved using a 1-D Fokker-Planck equation to represent the collisional transfer of power to the thermal species. This collisional heating is added to the direct wave damping profiles to obtain the net power deposition profiles for the electrons and all ionic species as input heating source profiles in WHIST.

TRANSPORT MODEL

The possible variations of transport coefficients is virtually limitless; we decided to rely on input from interpretive analyses of JET pellet plasmas for the particle transport and extend the values to energy transport using a simple approximation to theoretical relationships. The particle transport coefficients are taken from interpretive analysis of JET for shot 16211 during the enhanced confinement period.[8] To the neoclassical diffusive and Ware pinch terms, we add an anomalous diffusive term of the form:

$$\Gamma(\rho) = \Gamma^{nc} - D^{an}(\rho) \frac{\partial n(\rho)}{\partial \rho}$$

where $D^{an} = 0.08\text{m}^2/\text{s}$ in the core, rises sharply to $0.2\text{m}^2/\text{s}$ at $\rho/a = 0.4$, and then increases as ρ^2 to $0.4\text{m}^2/\text{s}$ at the plasma edge. The critical features are the low central value and the sharp rise. The increase in the outer portion of the plasma probably does not affect the calculations very greatly.

The heat fluxes are constructed in the same way; to the neoclassical terms we add an anomalous electron and ion conduction terms. The relationship between the anomalous electron conductivity and the anomalous particle diffusivity is taken as $\chi_e^{an}(\rho) = 13D^{an}(\rho)/4$ where the factor $13/4$ arises in the neoclassical quasilinear theory of fluctuation-induced transport.[6] We retain only the diagonal terms for simplicity. For the anomalous ion contribution we select as a reference $\chi_i^{an} = \chi_e^{an}$.

We retain the same values of the anomalous transport coefficients throughout the ohmic and heating phases, and both before and after pellet injection.

ANALYSIS OF JET SHOT 16211

JET shot 16211 exhibited the enhanced confinement characteristics and was selected as a reference shot for analysis. Figures 1 and 2 show the time history of many of the experimental discharge characteristics in the time interval 42 – 46 s. The results from a WHIST calculation are marked as x's in the time interval 42 – 44 s.

The total plasma current (Fig. 1a) was a programmed input to the WHIST calculation and reached the 3 MA flattop value at ≈ 43.5 s. The current profile was initialized such that the axial safety factor, q_o (Fig. 1a), matched the value determined by IDENTC at 42 s, and both q_o and the loop voltage at the plasma boundary then track well with the experimental values when evolved with neoclassical resistivity. The internal inductance shown in Fig. 1b is also a measure of the current profile shape and the simulation matches the IDENTC result. The ICRH power, Fig. 1c, was an input to the ray-tracing calculation; it rose abruptly to 5 MW at 43.2 s then increased approximately linearly to 7 MW at 44 s. The calculated ohmic power (Fig. 1c) shows an abrupt rise from 2 to 4 MW at the time of pellet injection, 43 s, then decays exponentially to about 1 MW at 44 s. The ohmic power from the magnetic analysis is somewhat smoothed over the pellet transient, but shows the essentially same behavior.

Modeling impurities and radiation with a predictive transport code to match experimental values of Z_{eff} and radiation is very difficult. We chose carbon, oxygen, and nickel in the density ratio 1.0:0.2:0.01 and the magnitude such that $Z_{eff} \approx 2$ at 43 s. Radiation losses are then evaluated with a coronal equilibrium model.[7] The impurity densities were kept constant through the WHIST simulation because of a lack of an option to program them in time, but this can be remedied for future calculations. When the pellet is injected, Z_{eff} decreases because of impurity dilution as shown in Fig. 1d. Both the visible bremsstrahlung and neoclassical resistivity analyses indicate the dilution effect but then show Z_{eff} rising, indicating a buildup of impurities after that. The bolometer measurement of radiative and charge-exchange loss (Fig. 1e) also shows

Figure 1: The time evolution of JET discharge characteristics with WHIST simulation values marked as x's: a) plasma current, central safety factor, and loop voltage; b) internal inductance; c) ICRH and ohmic power; d) Z_{eff} ; e) radiative and charge-exchange power loss; and f) energy confinement time.

Figure 2: The time evolution of JET discharge characteristics with WHIST simulation values marked as x's: a) total plasma particle content; b) axial electron density; c) axial electron temperature; d) axial ion temperature; e) total plasma kinetic energy; and f) D-D reaction rate.

Figure 3: WHIST simulation of the time evolution of electron density and temperature with experimental values marked as x's: a) axial electron and ion temperatures; b) axial electron density; c) electron temperature profile; and d) electron density profile. The ion temperature profile is essentially the same as the electron temperature profile.

impurity increase and at 44 s the loss calculated by WHIST is low by about 1 MW. Impurity radiation also affects the assessment of global energy confinement time. The WHIST simulation shows the energy confinement time rising from a prepellet ohmic value of 0.3 s to 0.75 s at 43.5 s and then holding there until 44 s. This increase is purely a geometric effect from the strongly peaked axial ICRH heating[9] because there is no density, temperature, or power scaling in the transport coefficients. On the other hand, the diamagnetic analysis indicates the confinement time dropping again to about 0.4 s at 44 s. This is at least in part due to the increased radiation loss, and may be amplified if that loss is strongly peaked in the plasma center.

The total plasma electron content (Fig. 2a) rises in the ohmic phase even in the absence of gas puffing. We model this in WHIST with 70% direct particle recycle plus a virtual particle source representing a slow release of the wall particle inventory. The total source of $\approx 10^{21}$ s in the WHIST simulation is in reasonable agreement with H_α measurements and exceeds the diffusive plus charge exchange losses. The increase in particle content at 43 s was modeled with a deuterium pellet of effective spherical radius $r_p = 2.23$ mm, representing 92% of the ideal mass of a 4.0 mm diameter and length cylinder. The initial decay of the particle content after pellet injection is modeled with the same 70% recycle and virtual source. The saturation at higher density can only be modeled with increased hydrogenic and impurity sources associated with the additional plasma heating. Pellet penetration and the resulting particle source profile were

calculated with the neutral and plasma shielding model.[10] In the calculation, pellet penetration was short of the axis while in the experiment it penetrated to the axis. Calculated ablation rates are not very reliable close to the axis because of the singularity in the plasma volume. The calculated axial density rise was slightly higher than that given by inversion of the FIR chords (Fig. 2b) but decays at the same rate as observed experimentally. The axial electron and ion temperatures show excellent agreement over the entire time interval from 42 – 44 s (Fig. 2c-d). The ICRH ray-tracing calculation indicated comparable total electron and ion heating rates with an H minority fraction of $n_H/n_e \approx 2.5\%$; since T_{eo} and T_{io} were observed to rise at the same rate we chose to use the same anomalous conductivities for electrons and ions. The relative ion and electron heating rates are sensitive to the minority fraction, which is not well known, so definitive conclusions about the split between anomalous electron and ion losses cannot be made. In simulations extending beyond 44 s we found the temperatures continued to rise. We expect the experimental saturation is due to impurity accumulation, both through radiation and reduction in the deuterium fraction (the deuterium fraction is an important factor in deducing T_{io} from neutron signals). Until 43.5 s the calculated total kinetic energy content agrees with the diamagnetic value (Fig. 2e). Increased radiation losses of 1 MW over the next 0.5 s (Fig. 1e) can explain the 0.5 MJ difference at 44 s. The neutron signal saturates at ≈ 43.7 s while the calculated value continues to rise (Fig. 2e); the saturation is likely due to a reduction in the deuterium content in the core as discussed earlier.

Axial temperatures and densities as well as the evolution of the electron temperature and density profiles from the WHIST simulation are shown in Fig. 3. The bump in the axial temperatures (Fig. 3a) is an artifact of the frequency of recalculating the ICRH deposition profile. Initially the resonance is located right at the magnetic axis. This very strong axial heating profile is held for about 0.2 s before being recalculated. By that time the outward shift of the axis has increased by ≈ 5 cm and the resonance no longer passes through the axis. The response of the axial density in the WHIST simulation is slower than observed (Fig. 3b) because the pellet did not quite reach the axis in the calculation. Once filled in, the axial density overshoots the experimental value. This could indicate that the calculated deposition profile is skewed a little too much toward the end of the pellet life. The electron temperature is very narrow (Fig. 3c) because of the central heating and low conductivity in the core. The ion temperature profile (not shown) has essentially the same shape. The hole in the center of the density profile from incomplete pellet penetration can be seen in Fig. 3d. The profile fills in rapidly then exhibits the characteristic central hump of deep pellet fueling with a broad outer shoulder.

CONCLUSIONS

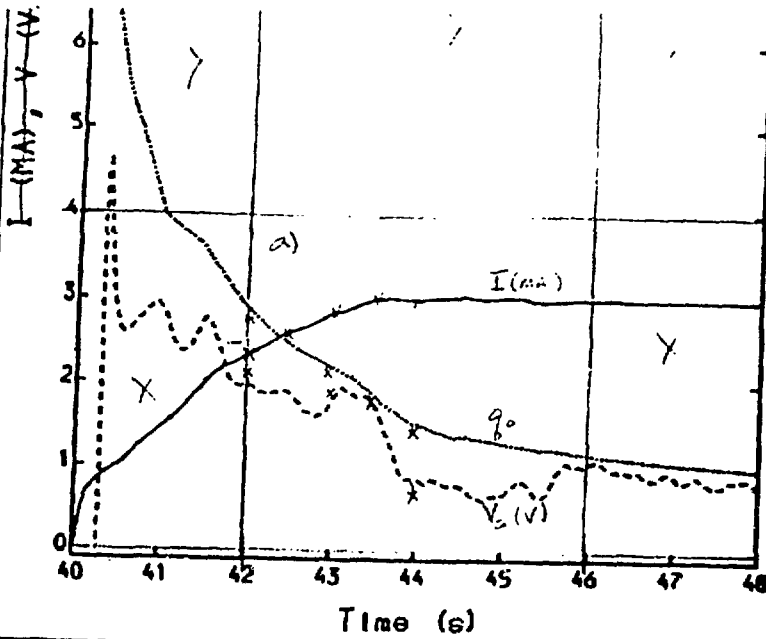
ICRH heating of highly peaked density profiles associated with deep pellet fueling leads to a period of enhanced confinement. During this period, the plasma behavior can be modeled with the same transport coefficients as in the ohmic plasma. The enhanced confinement comes mostly from the geometric effect associated with strong central heating, and begins to deteriorate as impurity radiation increases.

REFERENCES

- [1] G. L. Schmidt, et al., to be published in *Plasma Physics and Controlled Nuclear Fusion Research* (Proc. 12th Int. Conf., Nice, 1988).
- [2] D. Q. Hwang, C. F. F. Karney, J. C. Hosea, "Modeling of ICRF Heating of a Tokamak

Plasma," Princeton Plasma Physics Laboratory Report, PPPL-1990 (1983).

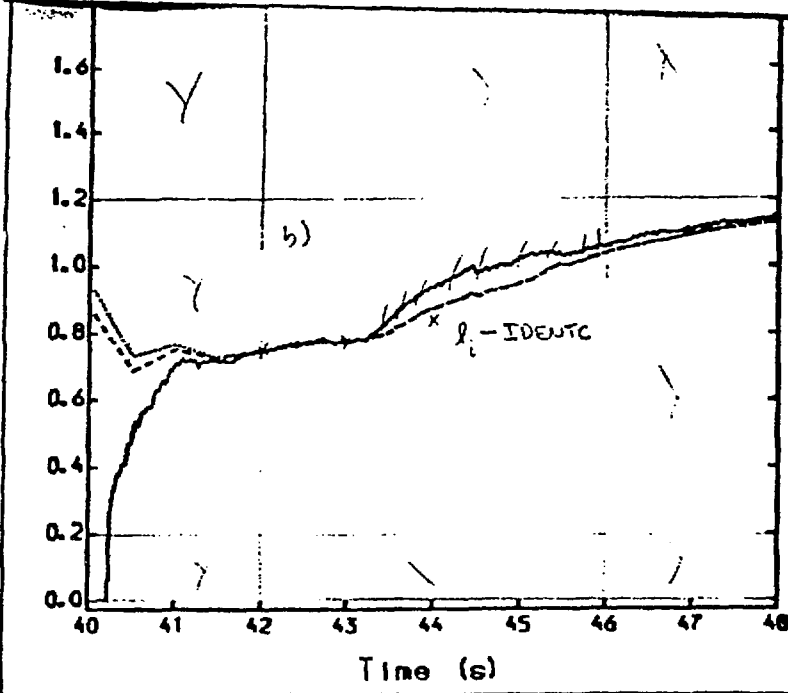
- [3] D. G. Swanson, S. Cho, C. K. Phillips, D. Q. Hwang, W. Houlberg, L. Hively, *Plasma Physics and Controlled Nuclear Fusion Research* (Proc. 11th Int. Conf., Kyoto, 1986), Vol.1, IAEA, Vienna (1987) 653.
- [4] I. B. Bernstein, *Phys. Fluids* 18 (1975) 320
- [5] C. F. Kennel, F. Engelmann, *Phys. Fluids* 9 (1966) 2377.
- [6] K. C. Shaing, *Phys. Fluids* 31 (1988) 2249.
- [7] D. E. Post, R. V. Jensen, C. B. Tarter, W. H. Grasberger, W. A. Lokke, *Atomic Data and Nuclear Tables* 20 (1977) 397.
- [8] L. R. Baylor, et al., this conference.
- [9] J. D. Callen, J. P. Christiansen, J. G. Cordey, P. R. Thomas, K. Thomsen, *Nucl. Fusion* 27 (1987) 1857.
- [10] W. A. Houlberg, S. L. Milora, and S. E. Attenberger, *Nucl. Fusion* 28 (1988) 595.



~~VOLTAGE AT PLASMA BOUNDARY~~
~~NO.~~
~~(MG2 VSU)~~ • -1.0
~~OE+00)~~
~~AXIAL 0 (PSI)~~
~~(IDC2 OAX)~~ • 1.0
~~OE+00)~~

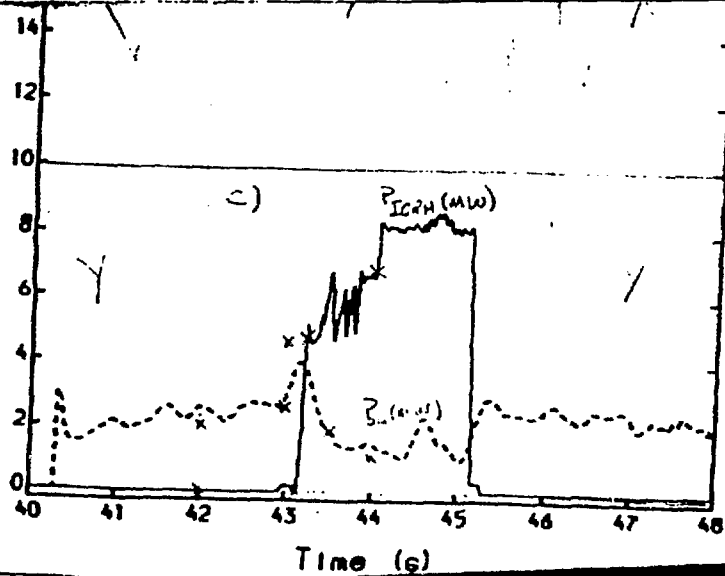
NTIPL0T 15.55.21 31/08/88

Fig 1



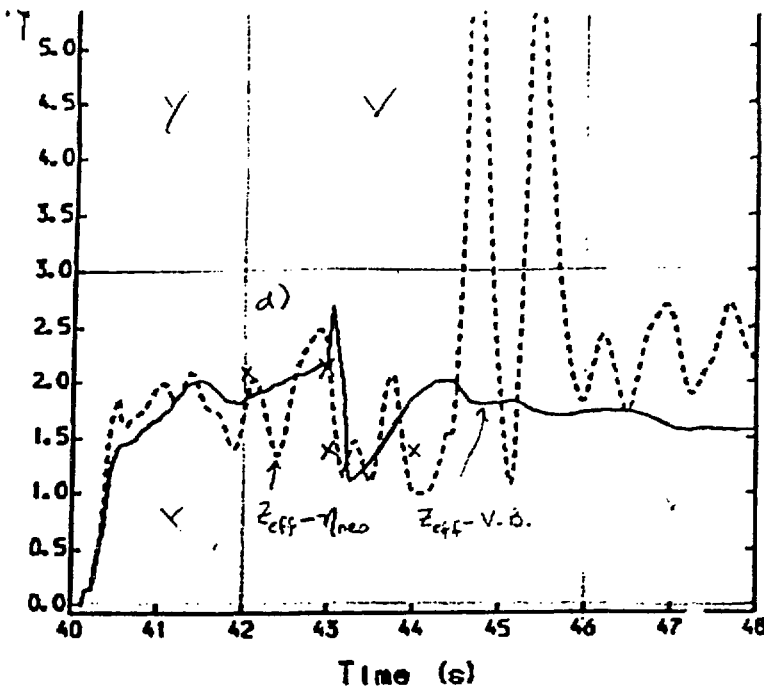
~~OE+00)~~
~~INTERNAL INDUCT. (IDENT)~~
~~(IDC2 INDI)~~ • 1.0
~~OE+00)~~
~~INTERNAL INDUCTANCE~~
~~(IDC2 XLI)~~ • 1.0
~~OE+00)~~

NTIPL0T 15.55.22 31/08/88



~~UT~~
~~(MG2 YOH)~~ • 1.0
~~OE-06)~~

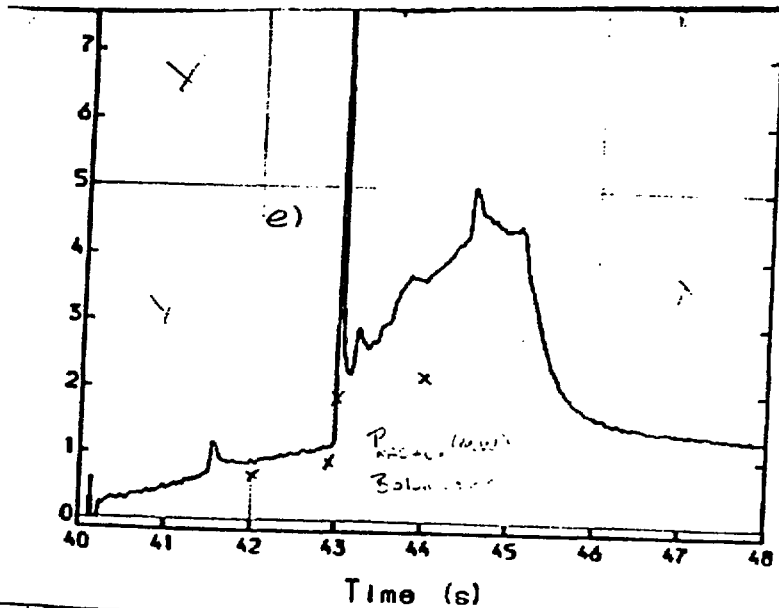
NTIPL0T 15.55.27 31/08/88



~~L₁
 (HAL EFZ • 1.0
 0E+00)
 --- ZEFF FROM RESIST. NEO
 CL.
 (KIN REQ • 1.0
 0E+00)~~

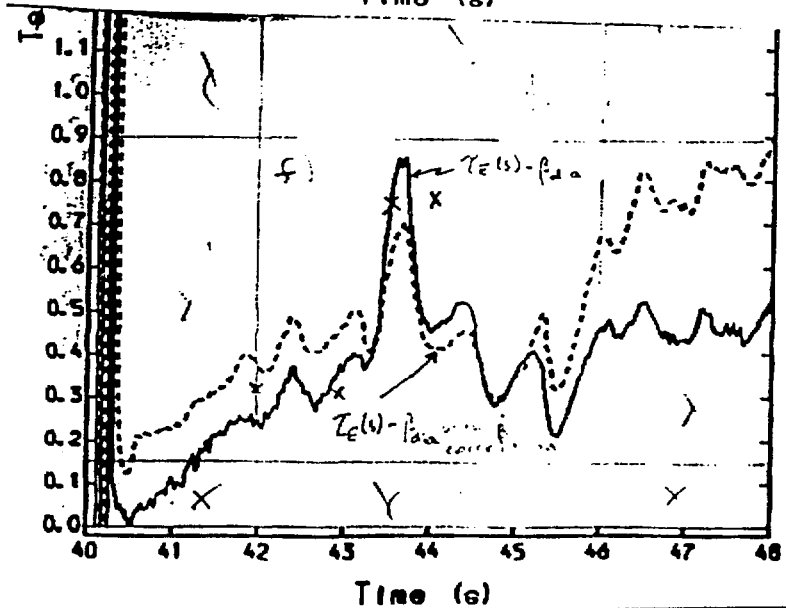
D

NTIPL0T 15.55.29 31/08/88



S

NTIPL0T 15.55.29 31/08/88



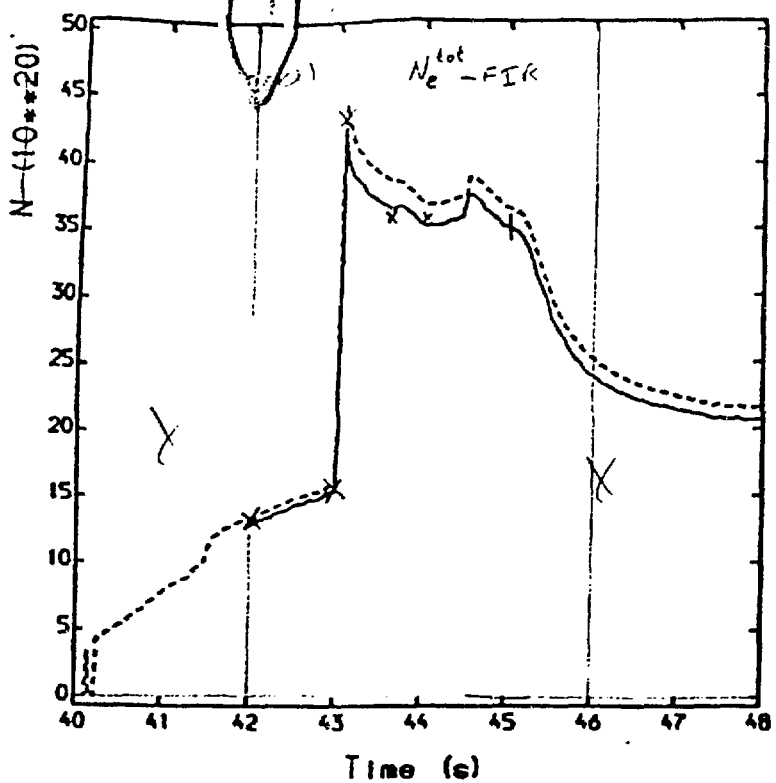
--- TAUE INCL. D/DOT/DOT/TAU
 (MG2 TUC • 1.0
 0E+00)

REPRODUCED FROM
BEST AVAILABLE COPY

NTIPL0T 15.55.27 31/08/88

F.51

total electrons

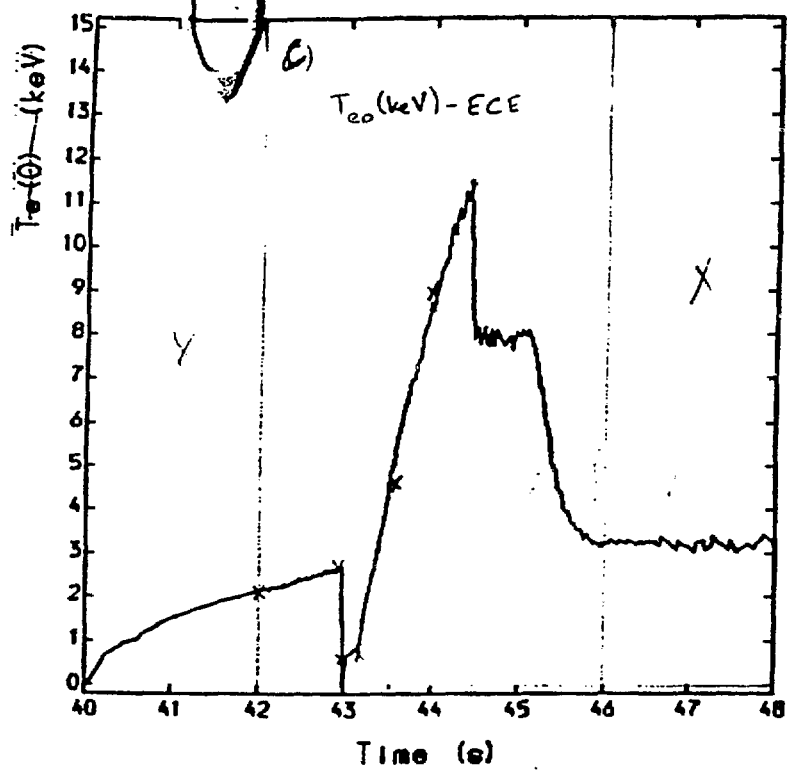


SYMBOL TABLE	
—	VOLUME INTEGRATED NE (NEPR NEV 21 • 1.0 OE-20)
- - -	PARTICLE INVENTORY NT OT (HAL TON • 1.0 OE-20)

D

NTIPL0T 15.55.24 31/08/88

Central Electron Temperature



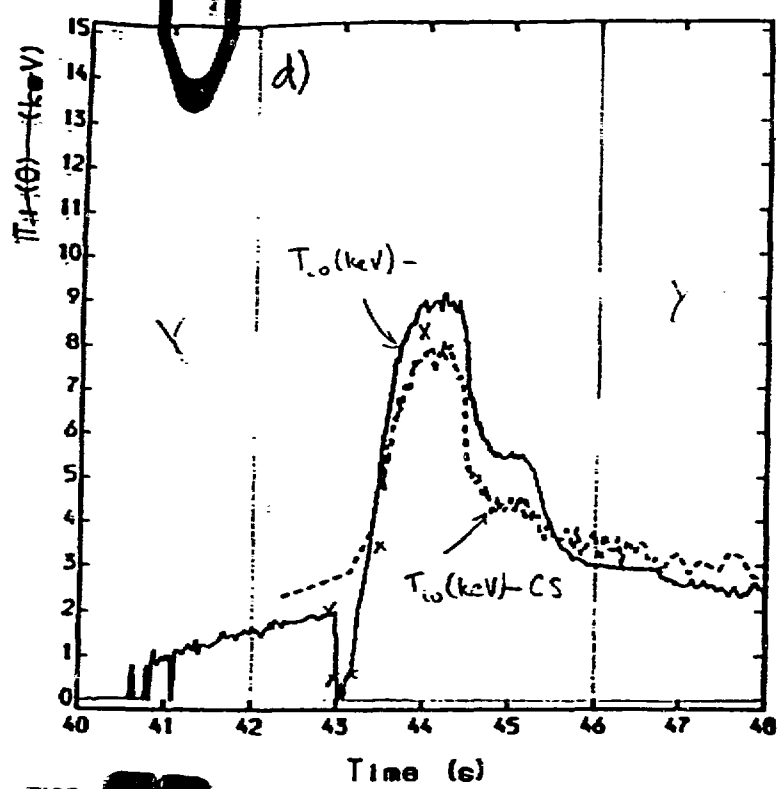
SYMBOL TABLE	
—	MAXIMUM TEMPERATURE (ECH1 MAX • 1.0 OE-03)

S

NTIPL0T 15.55.25 31/08/88

Fig 2

Central Ion Temperature



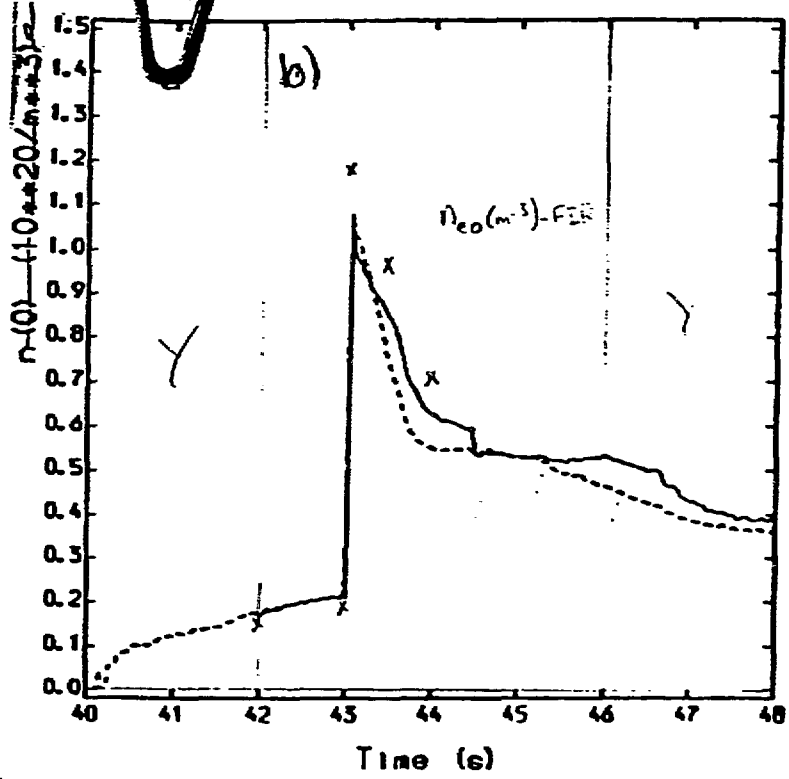
SYMBOL TABLE	
—	AXIAL ION TEMPERATURE (TIN / IIX • 1.0 OE-03)
- - -	TI FROM KXI VOIGT FIT (XCS TI • 1.0 OE-03)

(9)

NTIPL0T 15.55.26 31/08/88

Central Electron Density

SHOT 16211

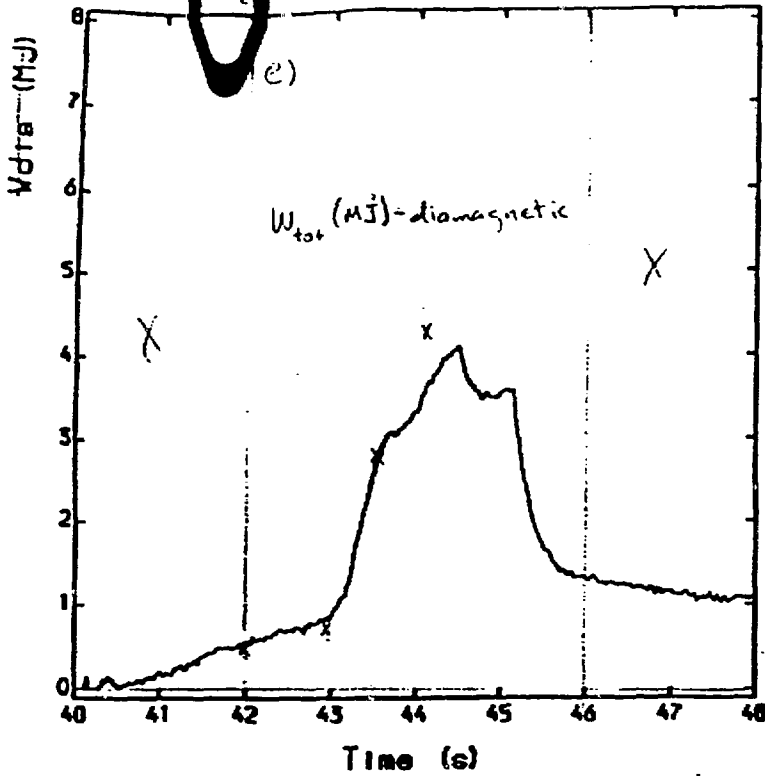


SYMBOL TABLE	
—	NE(t) ON A FIXED MESH (NEPR PRFL 21 • 1.0 OE-20)
- - -	AXIAL PLASMA DENSITY (NEX AX • 1.0 OE-20)

(10)

NTIPL0T 15.55.23 31/08/88

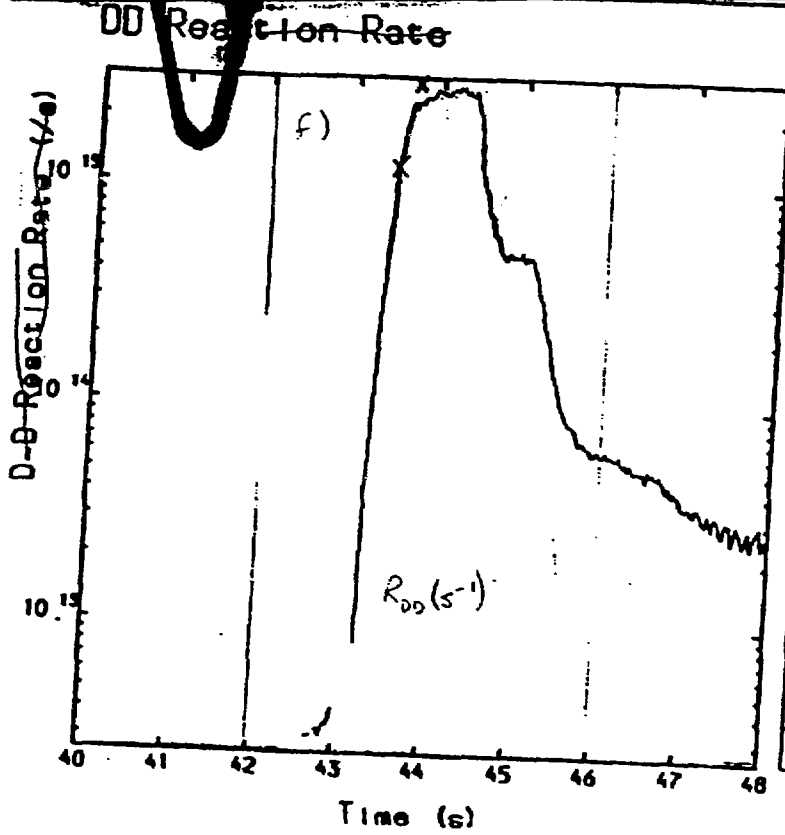
Fig 2



SYMBOL TABLE	
—	TOTAL PLASMA ENERGY D
	IAM
	(MG3 / VPD) • 1.0
	OE-06/1

(11)

NTIPL0T 15.55.26 31/08/88



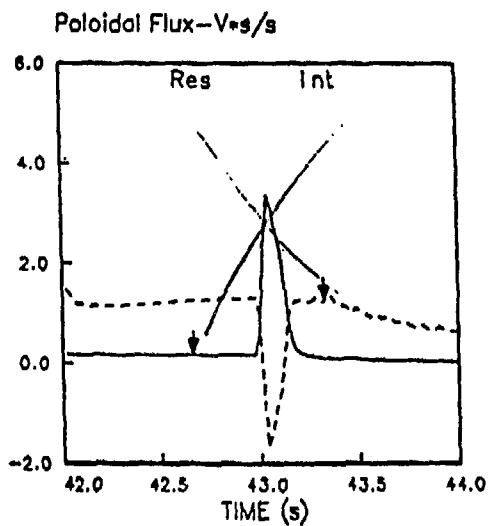
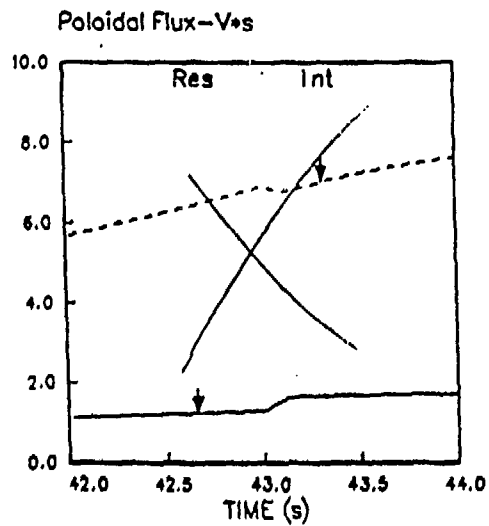
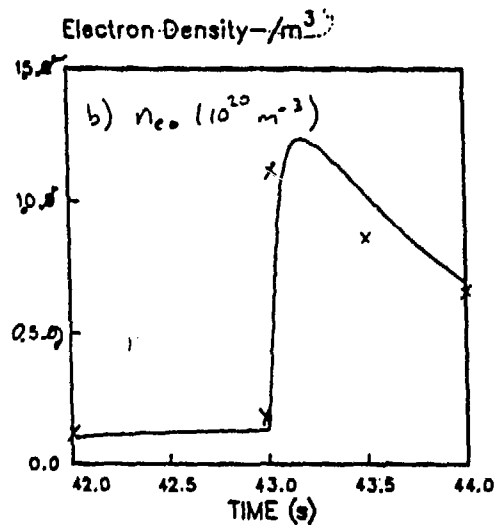
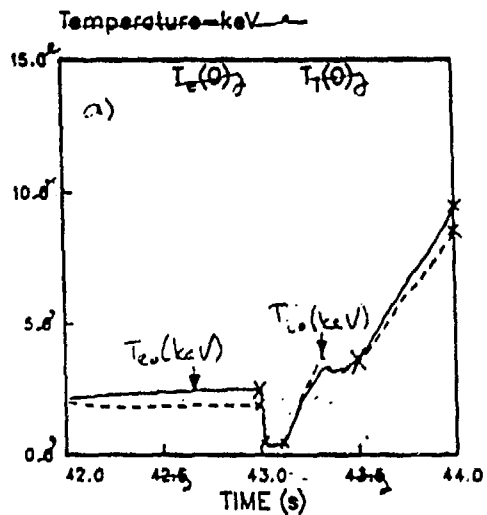
SYMBOL TABLE	
—	TOTAL D-D REACTION RA
	TE
	(TIN / RDD) • 1.0
	OE+00)

(12)

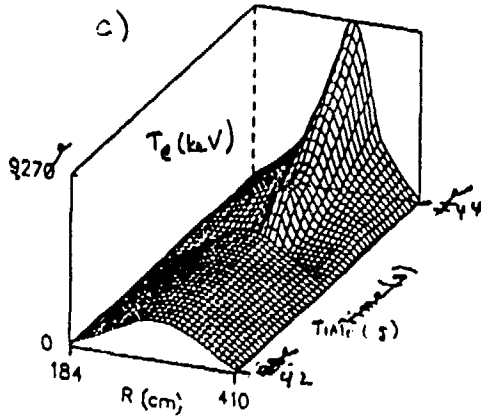
NTIPL0T 15.55.25 31/08/88

F: 5²

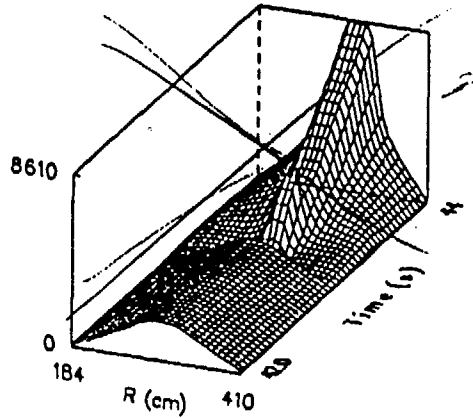
170³



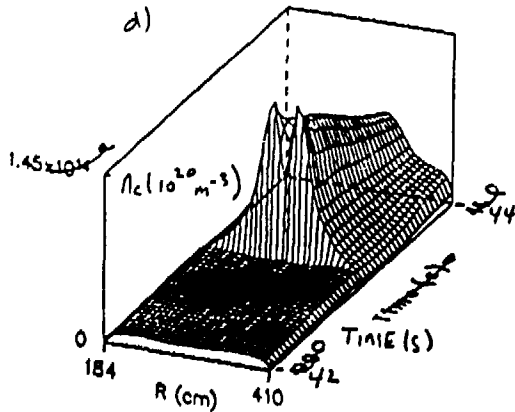
electron-temp. (ev) - a



ion temp. (ev)



electron-dens (/cm3) - a



ion dens(1) (/cm3)

